Interfacial Structure and Proton Conductivity of Nafion at the Pt-deposited Surface

Yutaro Ono and Yuki Nagao*

School of Materials Science, Japan Advanced Institute of Science and Technology,

1-1 Asahidai, Nomi, Ishikawa 923-1292 Japan

Abstract

Understanding the Nafion-Pt interface structure is important because fuel cell reactions occur at the three-phase boundary. Infrared (IR) p-polarized multiple-angle incidence resolution spectrometry (p-MAIRS) technique was used to investigate the in-plane (IP) and out-of-plane (OP) spectra in the identical substrate. Our previous study revealed that the proton conductivity of the Nafion thin films decreased at the MgO and SiO_2 surfaces. We proposed that the origin for the lower proton conductivity can be derived from the highly oriented structure at the interface. However, the interface structure of the Nafion-Pt interface remains unclear. In this study, Nafion thin films were prepared by spin-coating on a Pt-deposited MgO substrates. The IP spectrum exhibited a well-known spectrum, but the OP spectrum was quite differed considerably from the IP spectrum. Furthermore, thickness dependence of the degree of orientation for this OP band was observed at the Nafion-Pt interface. This OP band can be assigned as the vibration mode of the mixture of the CF_2 and sulfonic acid groups. At the

low-RH region, proton conductivity of the Nafion thin film on the Pt-deposited surface was one order of magnitude higher than that on the SiO_2 surface. Furthermore, the activation energy was 0.4–0.5 eV, which is lower than that of the SiO_2 surface. These results, which suggest that the Pt surface influenced the proton transport property of Nafion thin film, can contribute to understand the relationship between the proton transport property and thin film structure on the Pt-deposited surface at the three-phase boundary for fuel cells.

1. Introduction

Polymer electrolyte fuel cells (PEFCs), which are anticipated for use as a next-generation power source, have been investigated extensively for use in energy conversion for automotive, portable device and other applications. The membrane electrode assembly (MEA) comprises a catalyst layer and the electrolyte membrane. Understanding this interface has become necessary because reactions occur at the three-phase boundary of a proton conductive ionomer, catalyst (Pt or Pt alloy), and gas. Therefore, the structure and properties of the materials at the interface must be elucidated [1]. Some reports have described that the interfacial confinement of polymer electrolyte structure strongly affects the proton transport property [2–6].

Nafion, the most well-known and widely studied ionomer developed by DuPont, has high proton conductivity in addition to excellent thermal and chemical stability [7]. The chemical structure of Nafion consists of a hydrophobic polytetrafluoroethylene (PTFE) backbone with perfluorinated ether side chains terminated by hydrophilic sulfonic acid groups, as shown in Scheme 1.

Scheme 1. Nafion structure.

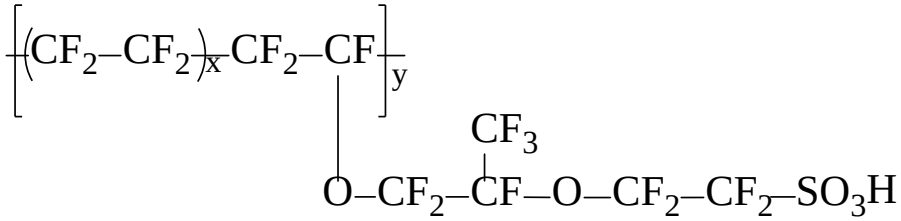

The structure in commercial bulk Nafion membrane has been investigated thoroughly using small-angle X-ray scattering technique [8–11]. A phase separation structure in hydrated Nafion has been reported. Moreover, Nafion is used in a solution state with various solvents for the preparation of MEA. The ideal ionomer layer in the MEA is regarded as extremely thin [12,13]. Paul *et al*. have reported the properties of ultrathin Nafion films [14–17]. The structure and properties of bulk Nafion membranes have been investigated widely in several studies described the literature, but the character of its confined thin film in the catalyst layer is still not well understood.

Several studies of Nafion thin films have been reported on the structure, water uptake, proton transport, and other characteristics. Neutron reflectivity (NR) [18–22], grazing incidence small-angle X-ray scattering (GI-SAXS) [23–27], and X-ray specular reflectivity (XRR) [28] techniques have revealed the effects of confinement and substrates. The NR study has revealed a lamellar structure between the SiO_2 substrate and Nafion thin film [19]. Moreover, a single hydrated layer appeared at the metal interface such as Pt and Au surfaces [18, 19]. Surface hydrophilicity and the water–vapor interface contributed to the structure of the Nafion surface [23, 24]. Results of another GI-SAXS study have demonstrated that the degree of the phase separation losses with decreasing the thickness [26]. Furthermore, Kusoglu *et al.* reported that the annealed films also exhibit the loss of microphase separation [27]. Our previous studies conducted using infrared (IR) p-polarized multiple-angle incidence

resolution spectrometry (p-MAIRS) technique [29, 30], which had been developed by Hasegawa [31–34], revealed the highly oriented molecular structure of Nafion thin films on both MgO(100) and Si wafer.

Some studies of proton transport have reported a decrease of the proton conductivity with decreasing thickness [16, 26, 30, 35], Moreover, proton conductivity has been described as quite lower than that of the commercial bulk Nafion membrane [15, 30]. Recent investigations have revealed that the hydrophilicity at the surface of Nafion ultrathin films is altered drastically by annealing, with conductivity changed by around one order of magnitude according to relative humidity [17].

Systematic analyses have examined the relationship between the structure and the proton conductivity of Nafion thin films. However, the relation between the interfacial behavior and proton transport property is not understood completely. For example, the different interfaces suggest the results of different water uptake [26, 27, 36–38]. Kongkanand reported that water uptake decreases concomitantly with decreasing the film thickness [36]. In contrast, Dishari *et al.* reported that the thin film at the SiO_2 interface had higher water uptake than thicker films [38]. These results suggest that the effects of the interface cannot be neglected. Bass *et al.* reported the surface hydrophilicity dependence of the micelle orientation [24]. However, proton conductivity has not been reported for the different interfacial conditions.

For use in fuel cell operations, the structure of confined Nafion thin films on a Pt surface has not been investigated sufficiently. As described herein, IR p-MAIRS technique was conducted to investigate the molecular structure of the Nafion thin films on Pt-deposited surface. IR p-MAIRS is increasingly regarded as a powerful spectroscopic tool for revealing molecular orientation in thin films. The p-MAIRS analysis showed that in-plane (IP) and out-of-plane (OP) transition dipoles are distinguishable in an identical infrared transparent substrate. However, because Pt is not transparent for IR light, we prepared an ultrathin Pt-deposited surface on the transparent substrate for p-MAIRS. This ultrathin Pt-deposited surface has enabled the measurement of proton conductivity because the electronic conductivity of the ultrathin Pt-deposited surface is lower than the proton conductivity of the Nafion thin film. This result can help to understand the relation between the proton transport property and the thin film structure on the Pt-deposited surface at the three-phase boundary for fuel cells.

2. Experimental

2.1 Nafion Thin Film Preparation on Pt Modified Surface

For this study, MgO (Furuuchi Chemical Industries Corp., Japan) and SiO_2 substrates (each 15 × 15 × 0.5 mm) were used respectively for IR and proton conductivity measurements. This study examined the relation between the thin film structure and proton conductivity on the

Pt-deposited surfaces that had been prepared on each substrate using radio frequency (RF) magnetron sputtering system (KXS-110; Kenix Co. Ltd.). First, Pt-deposited surfaces were prepared by RF sputtering of a pure platinum (99.99%, Kojundo Chemical Laboratory Co. Ltd.) metal target. The RF power was applied, 20 W and 15 W respectively to MgO and SiO_2 substrates. Deposition was done in 20 s at room temperature with an Ar atmosphere. To obtain thin film thickness of Pt layer, deposition parameters were optimized. The thickness of the Pt-deposited layer was c.a. 15–20 nm (Figure S1), determined using atomic force microscopy (AFM, VN-8000; Keyence Co.). The Pt-deposited surface was characterized using X-ray photoelectron spectroscopy (XPS, AXIS-ULTRA DLD; Shimadzu Corp.). As a reference, MgO and SiO_2 substrates were used without Pt deposition. Before using them, plasma cleaning (Cute-MP; Femto Science, Korea) was conducted.

For thin film preparation by spin-coating (ACT-200; Active Co. Ltd.), 5 % Nafion dispersion (DE521 CS type; Wako Pure Chemical Industries Ltd.) was used. Thicknesses of 20–400 nm were found using a surface profiler (P-15; KLA-Tencor Corp.). The thickness was controlled by adjustment of the Nafion solution concentration using ethanol and water. The Nafion thin films were dried for at least 12 hr in a desiccator.

2.2 Infrared (IR) p-polarized Multiple-angle Incidence Resolution Spectrometry (p-MAIRS)

To investigate IP and OP molecular vibrations in an identical thin film, the IR p-MAIRS technique was performed. The p-MAIRS measurements were taken using an FT-IR spectrometer (Nicolet 6700; Thermo Fisher Scientific Inc.) equipped with a mercury–cadmium–telluride (MCT) detector. The optical configuration is shown in Figure 1. To obtain the p-polarized light, a ZnSe polarizer was used. Single-beam spectra were collected from 38° through 8° in 6° steps between the angles of incidence. The wavenumber resolution was 4 cm^{-1}. The number of scans was 64 for each angle of incidence. Dry air or N_2 gases passed through the sample compartment and inside of the spectrometer for air purge. The humidity of the sample compartment was less than 5% under room temperature. The aperture was fully opened (size of 150). A metal plate with small pores was placed in the light path of the incidental beam to prevent saturation. The p-MAIRS analysis from the collected spectra was conducted automatically using p-MAIRS analyzer software (Thermo Fisher Scientific Inc.).

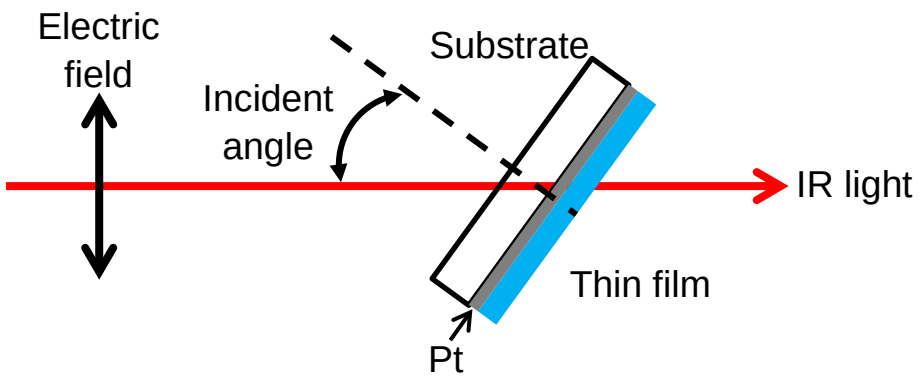

Figure 1. Configuration of the polarized incident beam path and incident angle.

2.3 Proton Conductivity Measurement of the Nafion Thin Films

The proton conductivity of thin films was measured at relative humidity (RH) range of 40–95% and temperature of 298–333 K using an impedance / gain-phase analyzer (SI1260; Solartron Analytical) with a dielectric interface system (SI1296; Solartron Analytical) with humidity-controlled and temperature-controlled chamber (SH-221; Espec Corp). Measurements were taken parallel to the substrate. The Au electrodes were fabricated at the edge of thin film. The impedance data were collected at the frequency range of 10 MHz and 1 Hz with amplitude of 50 mV. Proton conductivity (σ) was calculated as follows,

$$\sigma = \frac{d}{Rlt} \qquad (1)$$

where d is the distance between the Au electrodes, R is the resistance value from impedance, l and t are the length of the contact electrodes and thickness of the film respectively.

2.4 DFT Calculations

For the attribution of IR spectra, density functional theory (DFT) calculations were performed using the DMol3 package in Materials Studio (Accelrys Software Inc.). The Perdew−Burke−Ernzerhof (PBE) function was chosen. Convergence threshold for the maximum force and maximum displacement for normal geometry optimization were set respectively to 0.004 Ha $Å^{-1}$ and 0.005 Å.

3. Results and Discussion

The p-MAIRS technique has never been applied to the Pt-deposited surface. To confirm the validity of the p-MAIRS technique using a Pt-deposited surface on the MgO substrate, a validity check was carried out according to the literature [33]. Figure S2 shows the single-beam spectra with different incident angles. The intensity of the single-beam in the case of thicker Pt-deposited substrate was almost zero. However, the intensity for the thin Pt-deposited MgO (Figure S2(b)) was only 10% lower than that of the bare MgO substrate (Figure S2(a)). Each spectrum had a similar shape in the case of Pt-deposited and bare MgO substrates. The intensity of the single-beam spectra gradually decreased when the angle of incident decreased from 38° to 8°. Therefore, we inferred that this p-MAIRS technique is applicable with the Pt-deposited surface. To confirm the reproducibility for Pt deposition, Figure S2(c) shows the Pt-deposited MgO surface of three samples at 38°. The three samples

show similar spectra. The single-beam spectra of the SiO_2 showed different spectra compared to the MgO substrate, because SiO_2 has low IR transmittance (Figure S2(f)) as a result of the large absorption band at less than ca. 2100 cm^{-1}. The intensity from 4000 to 2200 cm^{-1} for thin Pt-deposited SiO_2 (Figure S2(e)) was a 4–10 % decrease compared with the bare SiO_2 substrate (Figure S2(d)). This value is approximately equal to that of the Pt-deposited MgO.

For Pt, an electroconductive material, the direction used for the impedance measurement is parallel to the Pt-deposited surface. For thick Pt thin film, proton conductivity cannot be measured because the resistance of Pt and Nafion thin films should be regarded as a parallel circuit. Therefore, a thin Pt-deposited surface is necessary to evaluate proton conductivity. Figure S3 shows the RH dependence of the resistance of Pt-deposited surface on the SiO_2 substrate. The resistance of the Pt-deposited surface was found to be independent of the RH: it was 10^{11} ohm. In contrast, the resistance of the 20-nm-thick Nafion thin film deposited on Pt / SiO_2 substrate was strongly dependent on the RH. The resistance of the Pt-deposited surface was one order of magnitude higher than that of the Nafion thin films in the whole RH region. Therefore the proton conductivity can be evaluated in comparison to the Pt electronic conductivity. Two reasons for the higher resistance of the Pt-deposited surface are considered: the thin Pt-deposited surface is oxidized; alternatively, Pt is an island structure rather than a smooth thin film. To assess these possibilities, XPS was used. Figure S4 shows XPS spectra of Pt 4f and Si 2p electrons for the Pt / SiO_2 surface. The binding energies of Pt

$4f_{7/2}$, $4f_{5/2}$ electron peaks were found respectively to be 71.5 eV and 74.7 eV. These values show good agreement with those of Pt $4f_{7/2}$, $4f_{5/2}$ electron peaks that have been reported in the literature [39]. The oxidation state of Pt 4f peaks was observed in curve-fitted XPS spectra (Figure S5). The relative peak areas were, respectively, ca. 25% (Pt^{+2} $4f_{5/2}$) and 75% (Pt^{+0} $4f_{5/2}$), respectively (Table S1). This result suggests that the Pt-deposited surface was partially oxidized. The Si 2p electron peak can be assigned as SiO_2. It can be supposed that the Pt-deposited surface has an island shape on the SiO_2 substrate. The surface morphology of the bare surface and Pt-deposited surface was obtained using AFM. Figure S6 shows topographic AFM images of the bare surface and Pt-deposited surface. Each image shows a 10 μm × 10 μm area of the surface. The smooth surface images were obtained respectively from bare MgO and SiO_2 surfaces in Figure S6(a) and S6(b), respectively. In contrast, rougher surfaces compared to bare surface were observed in both Pt-deposited MgO and SiO_2 surfaces, as shown in Figure S6(c) and S6(d). These results support that the Pt-deposited surface has island morphology on both substrates.

Figure 2 shows the incident angle dependence of the transmission IR spectra of the 300-nm-thick Nafion film on the Pt-deposited surface. The absorbance around 1260 cm^{-1} depended on the incident angle. This result suggests that the thin film has an oriented structure. For a low incident angle, the peak around 1260 cm^{-1} was not observed, which suggests that the IP transition dipole moment does not have so much. The shoulder peak

appeared gradually with the incident angle, meaning that OP transition dipole moments were excited by polarized light.

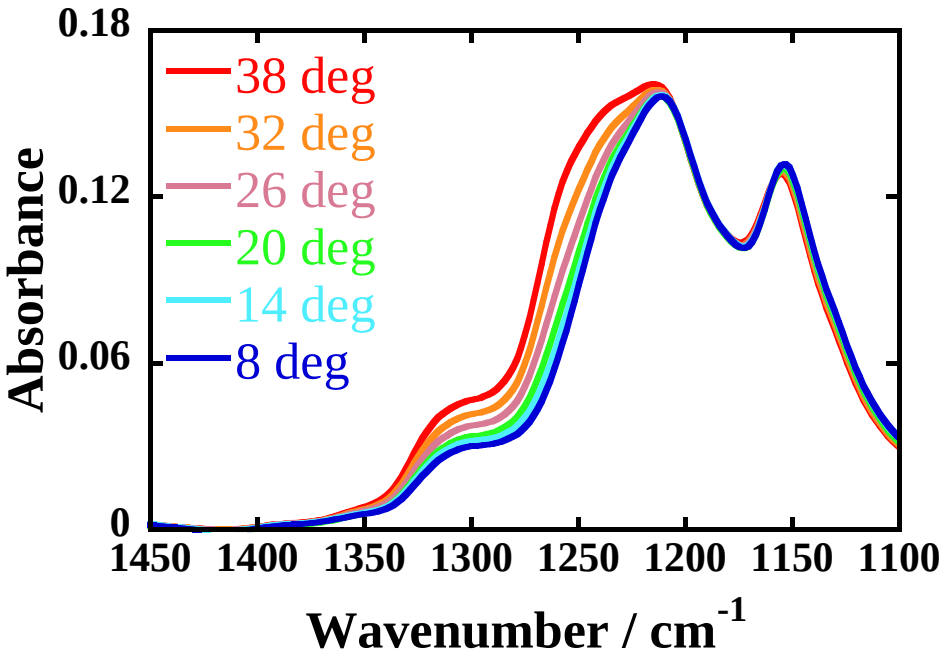

Figure 2. Incident angle dependence of the transmission IR spectra of the 300-nm-thick Nafion film on the Pt-deposited surface.

To discuss the details of the molecular orientation, p-MAIR spectra after the collection of single-beam spectra are shown in Figure 3. The Nafion membrane consists of a hydrophobic PTFE backbone with perfluorinated ether side chains terminated by hydrophilic sulfonic acid groups. The IP spectrum shows the well-known spectrum of Nafion membrane [40, 41]. The bands at 1150 and 1210 cm^{-1} are assigned respectively to ν_s (CF_2) and ν_{as} (CF_2). The shoulder band at 1300 cm^{-1} is assigned to ν_{as} (CF_3). These vibration modes can be observed

in the IP spectrum. However, the OP spectrum differed greatly from the IP spectrum. The characteristic absorption band at 1260 cm^{-1} was observed only in the OP spectrum. Many investigations of IR spectra have been conducted using commercial Nafion films with several hundred or tens of micrometer order thickness. Two groups have reported this peak located at 1260 cm^{-1} experimentally by polarization modulation infrared reflection absorption spectroscopy (PM-IRRAS) [42, 43]. They assigned different attributions of the band at 1260 cm^{-1} as $\nu(CF_2)$ [42] and $\nu_{as}(CF_3) + \delta_s$ (COC) [43] vibration mode, respectively. Zeng *et al*. assigned $\nu_{as}(CF_3)$ vibration mode at the 1269 cm^{-1} in the Raman spectra [44]. Malevich *et al*. and Korzeniewski *et al*. assigned attributions of the band at 1250–1350 cm^{-1} and 1249–1275 cm^{-1} as $–SO_3^-$ from a deconvoluted IR spectrum [45, 46]. In our previous report, this IR band at 1260 cm^{-1} was attributed to $–SO_3H$ vibration modes between the two sulfonic acid groups with hydrogen bonds by the DFT calculation [30]. Similar calculation results have been reported by another group [47]. Their calculations suggest that the dimer structure of triflic acid shows absorption near the 1260 cm^{-1}. They assigned this band as SOH in-plane bending vibration mode. Furthermore, Warren and McQuillan assigned the measured band at 1255–1289 cm^{-1} as sulfonic acid groups of perfluoro(2-ethoxyethane) sulfonic acid [48]. For further consideration the attribution of this band, DFT calculations were conducted as a modified model. Figure 4 shows a perfluorinated sulfonic acid as a model compound of Nafion for DFT calculation. This study employed the new model based on the Nafion equivalent weight

with a longer backbone than that described in our previous report. Vibration analysis was performed after geometry optimization. In our previous calculation with the short main chain of perfluorinated sulfonic acid, the band at 1260 cm^{-1} had not been suggested [30]. However, the CF_2 mode around 1260 cm^{-1} was suggested in this work using the longer main chain. Therefore, the band at 1260 cm^{-1} can be assigned as the vibration modes of the mixture of the CF_2 and sulfonic acid groups. That abrupt conclusion for this attribution seems inappropriate: further investigation is needed for this attribution. The peak at 1060 cm^{-1} [49], which corresponds to sulfonic acid group, is helpful for this attribution. However, this IR region cannot be discussed because of IR absorption by the MgO substrate.

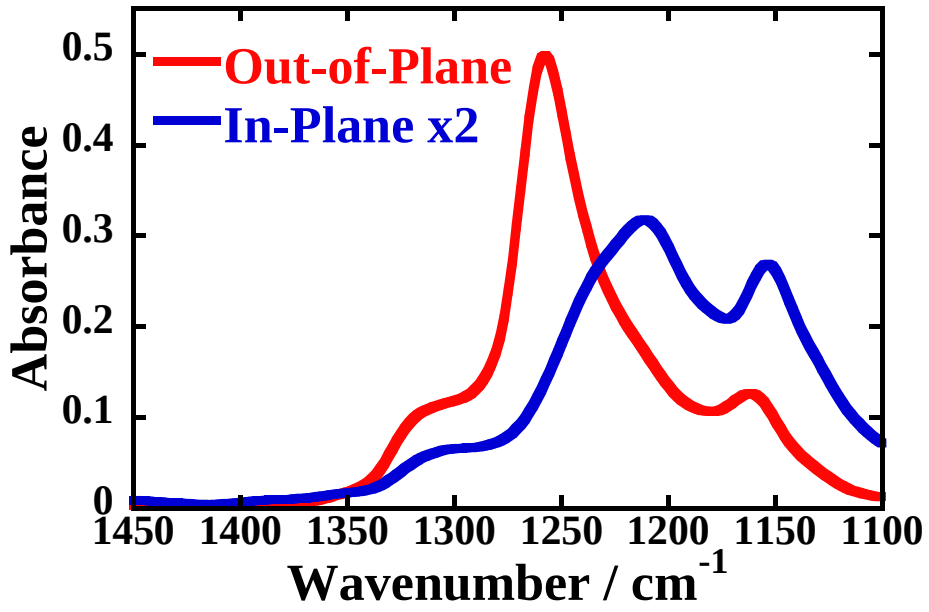

Figure 3. IR p-MAIR spectra of 300-nm-thick Nafion thin film on the Pt-deposited surface.

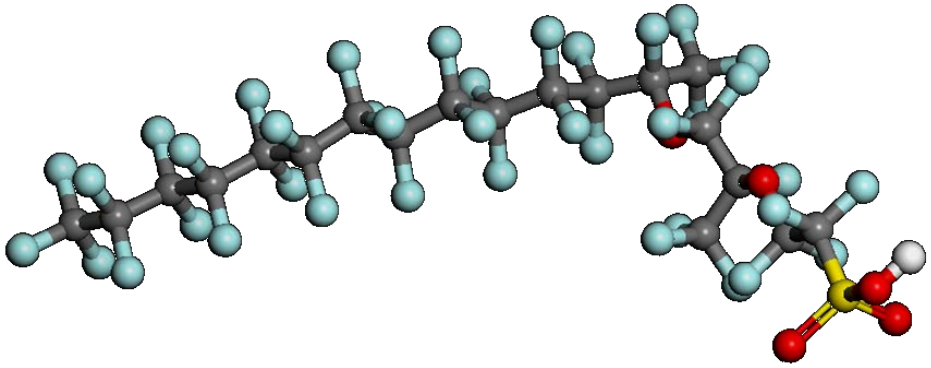

Figure 4. Nafion-like model for DFT calculation: carbon (gray), fluorine (light blue), oxygen (red), sulfur (yellow), and hydrogen (white).

Some literatures describe the thickness dependence by other measurements in the confined Nafion thin films. The proton conductivity [16, 26, 29, 35], water uptake [26, 27, 36–38], and degree of hydrophilicity depend on the thickness [14]. The thin film thickness may affect the interface structure. To investigate the interface structure of the confined Nafion thin films on

the Pt-deposited surface, Figure 5 shows the thickness dependence of the oriented structure on the Pt-deposited surface. The absorbance of the band at 1260 cm^{-1} depends strongly on decreasing thickness and decreases along with it.

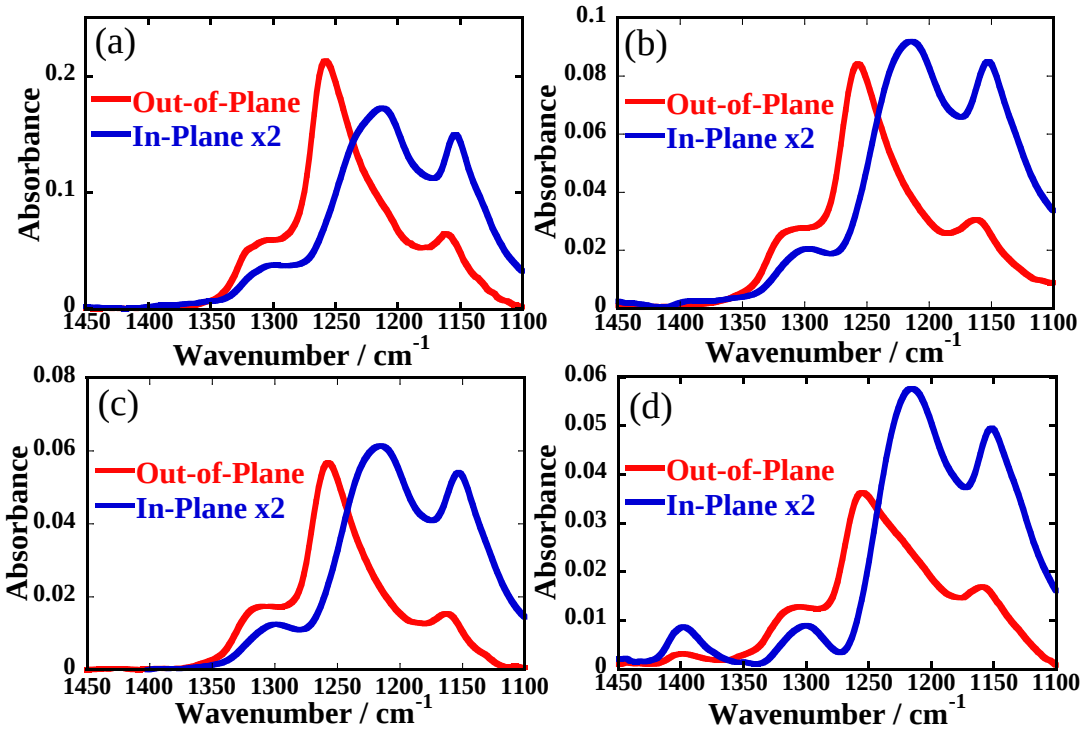

Figure 5. IR p-MAIR spectra of a Nafion thin film on the Pt-deposited surface. The thickness of Nafion thin films is (a)170 nm, (b)80 nm, (c)50 nm, and (d)35 nm thick.

Figure 6 depicts the thickness dependence of relative intensity ratios based on the strongest bands located at 1260 cm^{-1} (OP) and 1215 cm^{-1} (IP). The relative intensity ratio is calculated as follows,

$$Intensity\ ratio\ = \frac{I_{OP}(1260\ cm^{-1})}{I_{IP}(1215\ cm^{-1})} \qquad (2)$$

where I_{OP} and I_{IP} are derived from peak absorbance of IR p-MAIR spectra. The threshold was observed around 50–70 nm for the case of the Pt-deposited surface. The thin film structure changes drastically at this region of the thickness. A few literatures are available for the discussion between Pt and sulfonic acid groups [27, 44, 50, 51]. The possibility of a contribution by the difference of the surface morphologies between the Pt-deposited surface and MgO cannot be excluded based on our experimental results. And no apparent surface-enhanced IR effect was observed. The reason for the abrupt change in the intensity ratio remains under investigation. Additional information for the thin film structure can be considered at 1400 cm^{-1}. A new peak appeared for 35-nm-thick Nafion thin films on the Pt-deposited surface. This new peak can be assigned as (S=O) of the SO_3H [49]. Our model compound of Nafion also suggests the S=O and S-OH stretching modes of the -SO_3H groups at 1400 cm^{-1}. The dissociation state of the -SO_3H groups depends on the thickness. Although the proton of -SO_3H groups in the thicker thin film is dissociated, the proton of -SO_3H groups at the interface on the Pt-deposited surface is not dissociated in the dry atmosphere. The dissociation state might derive from the structure.

Thickness dependence has not been discussed for the previous case of the MgO substrate. Figure S7 shows the thickness dependence of the p-MAIR spectra. The absorbance did not depend as much as in the case of the Pt-deposited surface. As shown in Figure 6, thickness dependence of the intensity ratio between the Pt-deposited surface and MgO substrates showed a different trend. The threshold was not observed in the case of the MgO substrate which suggests that the thin film structure depends on the type of the substrate. Similar thresholds of the proton conductivity and surface hydrophilicity were reported respectively by Modestino *et al.* and Paul *et al.* using the thermal treated SiO_2 surface, [14, 26].

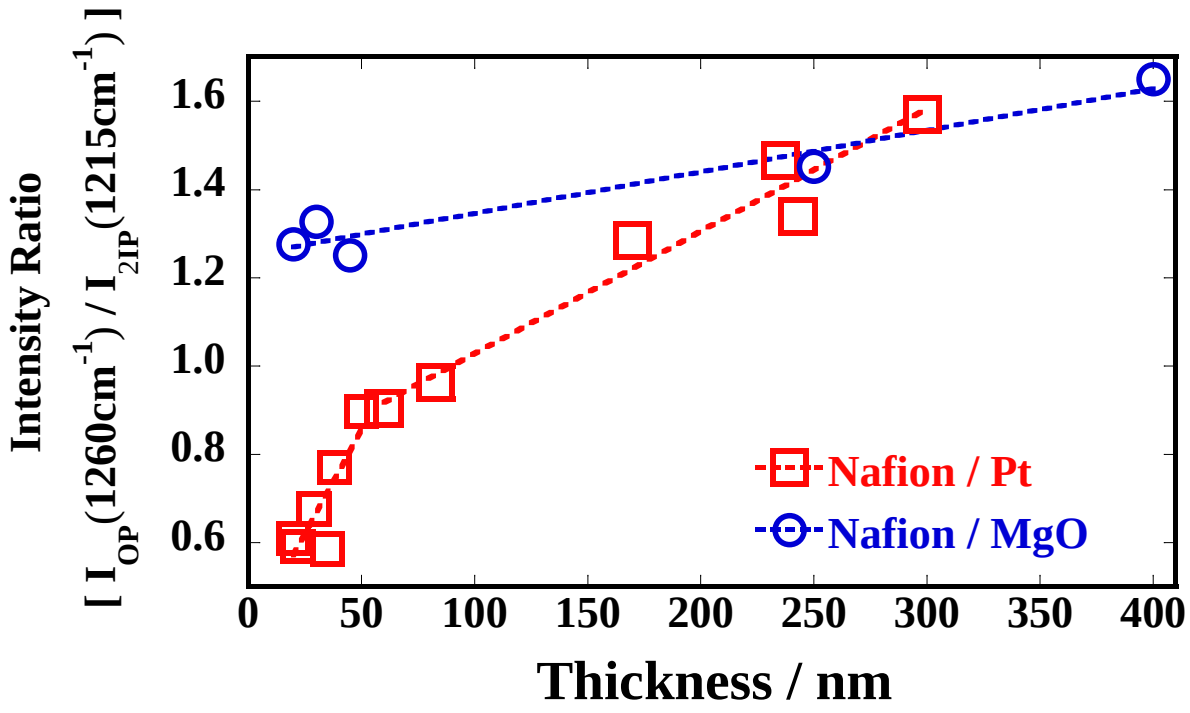

Figure 6. Thickness dependence of relative intensity ratios based on the strongest bands located at 1260 cm^{-1} (OP) and 1215 cm^{-1} (IP).

The thickness dependence of the proton conductivity on the SiO_2 substrate has been reported [16, 26, 29, 35]. Modestino and co-workers reported that this conductivity change derives from the change of the interface structure from the GI-SAXS results. However, the proton transport on the Pt-deposited surface has not been sufficiently discussed. The thickness dependence of proton conductivity of the Nafion thin film for various RH at 298 K is shown in Figure 7. Proton conductivity is dependent on thickness and RH. These proton conductivities were found to be $10^{-3} - 10^{-2}$ S cm^{-1} at 95% RH. However, their conductivities were lower than that of the commercial bulk Nafion membrane. Furthermore, stronger RH dependence of the proton conductivity was observed in the thin film case. At the low RH region, the proton conductivity depends on the surface type. Proton conductivity on the Pt-deposited surface was one order of magnitude higher than that on the SiO_2 substrate. This difference might derive from the different thin film structure and/or state of proton dissociation of the sulfonic acid groups, as discussed in the section of the p-MAIR results.

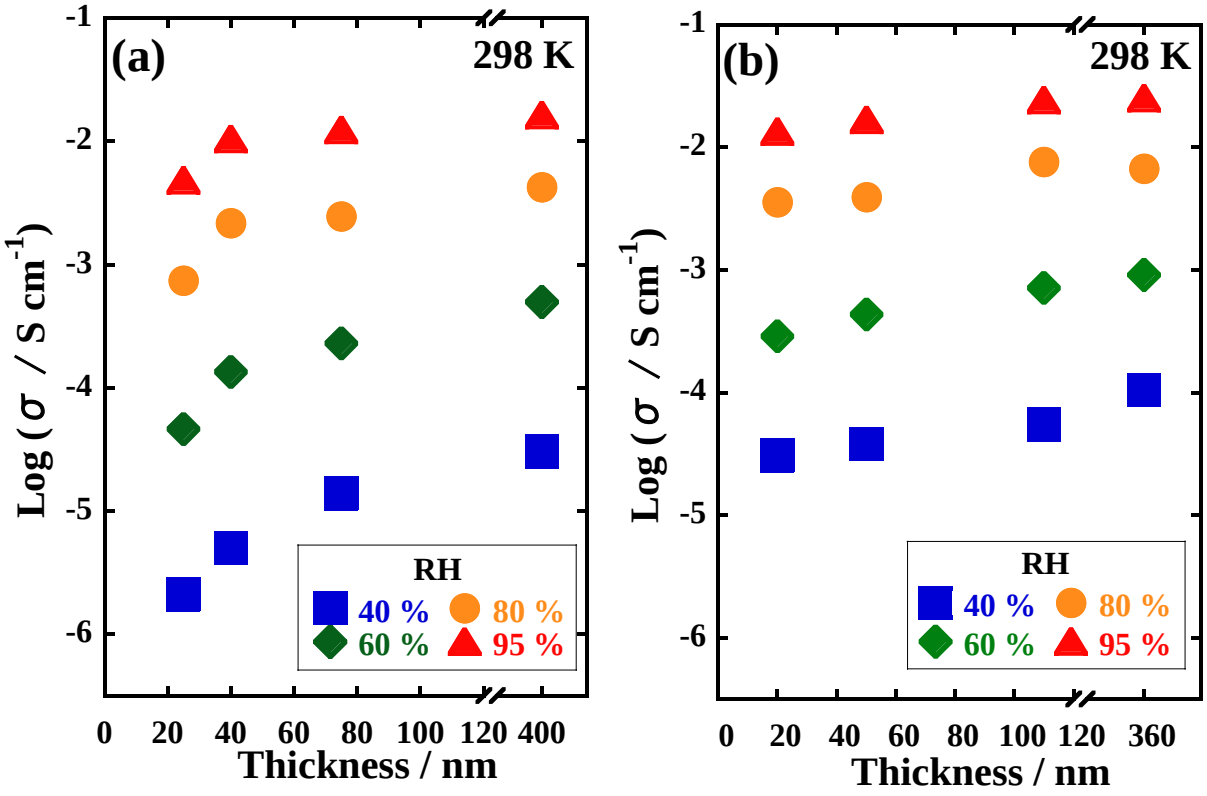

Figure 7. Thickness dependence of the proton conductivity for the Nafion thin films at various RH: (a) on SiO_2 and (b) on Pt-deposited surface.

The activation energy of each RH can provide useful information related to the proton conduction mechanism. To obtain the activation energy, the temperature dependence of the proton conductivity is shown in Figure S8. All log(σT) depended lineally on the $1000T^{-1}$ in this temperature region. The activation energy for the 40-nm-thick Nafion thin films on SiO_2 and Pt-deposited surfaces is shown in Figure 8 as a function of the RH. At the high RH region, all activation energies exhibited similar values (ca. 0.3–0.4 eV). However, at the low RH region, the activation energies depended strongly on the surface. The activation energy

depends strongly on RH in the case of the SiO_2 surface. A similar trend was reported by Paul *et al.* [16]. In the case of the Pt-deposited surface as new data, the activation energy was 0.4–0.5 eV, which has lower activation energy than in the SiO_2 surface case. The reason for the relatively higher proton conductivity at the low RH on the Pt-deposited surface is derived from this lower activation energy.

To understand the origin of the lower activation energy on the Pt-deposited surface, it is essential to consider the Nafion interface on the Pt-deposited surface. Water uptake and the diffusion coefficient of the water were informative physical parameters for the further discussion of the proton transport. Eastman *et al.* reported that the diffusion coefficient of the water decreased drastically at the interface [28]. These data are based on the PM-IRRAS with the Au surface and QCM measurements with the SiO_2 surface. The diffusion coefficient between the metal and SiO_2 surfaces shows no difference. Regarding water uptake, Murthi *et al.* and Kusoglu *et al.* reported that the water content (λ) at the interface on the Pt [18] surface is less than that of the bulk [27]. Modestino *et al.* reported that the water content at the interface on the SiO_2 surface is greater than that of the bulk. This greater water uptake enhances the dilution and isolation of the sulfonic acid groups. [26]. This contributes to the decrease of the proton conductivity and to the high activation energy. Based on the description presented above, the Nafion interface on the Pt-deposited surface might hold the low water contents. The appropriate amount of water might develop a favorable structure for

the proton conduction. The proton conductivity at further low RH around 0% was not obtainable because of limited machine specifications.

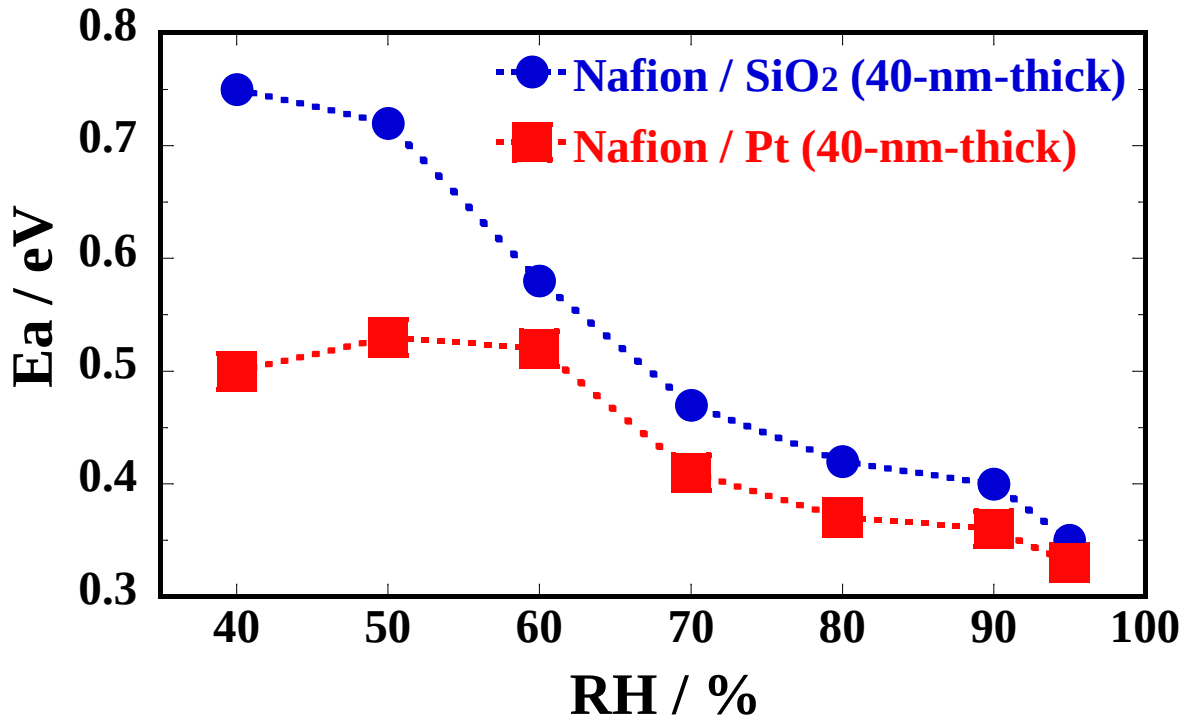

Figure 8. Activation energy for the 40-nm-thick Nafion thin films on SiO_2 and Pt-deposited surface as a function of the RH.

4. Conclusion

The interfacial confinement of polymer electrolyte structure strongly affects the proton transport property. Although structure and properties of Nafion bulk membranes have been investigated widely, the character of their confined thin films on the Pt-deposited surface as a model of the three-phase boundary remains unclear. Nafion has an orientation structure at the Pt-deposited surface by p-MAIRS. The degree of orientation on the Pt-deposited surface

depends on the thickness. A different dissociation state of sulfonic acid groups was also observed. At the low-RH region, proton conductivity depends on the Pt-deposited and SiO_2 surfaces. Proton conductivity on the Pt-deposited surface was one order of magnitude higher than that on SiO_2 substrate, but its conductivity remained lower than that of the bulk membrane. This difference might derive from the different thin film structure and/or the dissociation state of the protons at the sulfonic acid groups. For the Pt-deposited surface, the activation energy is 0.4–0.5 eV, which has lower activation energy than in the case of the SiO_2 surface. These results elucidate the relationship between the proton transport property and thin film structure on the Pt-deposited surface at the three-phase boundary for fuel cells.

Acknowledgments

The authors thank all reviewers to improve our manuscript. This work was financially supported by the Japan Society for the Promotion of Science (JSPS) through the Funding Program (GR060) for Next Generation World-Leading Researchers (NEXT Program), initiated by the Council for Science and Technology Policy (CSTP). This work was partially supported by research funds from the Ogasawara Foundation for the Promotion of Science and Engineering, The Kyoto Technoscience Center, and the Research Foundation for Electrotechnology of Chubu (REFEC).

ASSOCIATED CONTENT

Supporting Information

AFM image of cross-section of Pt-deposited surface, validity and reproducibility checks for p-MAIRS using Pt-deposited surface, RH dependence of the resistance of Pt-deposited surface and Nafion thin film, XPS spectra for Pt-deposited surface, AFM images of Pt-deposited and bare surfaces, thickness dependence of p-MAIR spectra, and Arrhenius plots for the proton conductivity of the Nafion thin films at various RH. These materials are available free of charge via the internet at http://pubs.acs.org.

AUTHOR INFORMATION

Corresponding Author

*ynagao@jaist.ac.jp Phone: +81(Japan)-761-51-1541, Fax: +81(Japan)-761-51-1149,

Address: 1-1 Asahidai, Nomi, Ishikawa 923-1292, Japan

Notes

The authors declare that they have no competing financial interest related to this study.

References

[1] Holdcroft, S. Fuel Cell Catalyst Layers: A Polymer Science Perspective. *Chem. Mater.* **2014**, *26*, 381–393.

[2] Nagao, Y.; Naito, N.; Iguchi, F.; Sata, N.; Yugami, H. Synthesis of Oligomeric Poly[(1, 2-propanediamine)-alt-(oxalic acid)] and Anomalous Proton Conductivities of the Thin Films. *Solid State Ionics* **2009**, *180*, 589–591.

[3] Nagao, Y.; Iguchi, F.; Sata, N.; Yugami, H. Synthesis and Proton Transport Property of Poly(aspartic acid) Thin Film on SiO_2 Substrate. *Solid State Ionics* **2010**, *181*, 206–209.

[4] Krishnan, K.; Iwatsuki, H.; Hara, M.; Nagano, S.; Nagao, Y. Proton Conductivity Enhancement in Oriented, Sulfonated Polyimide Thin Films. *J. Mater. Chem. A* **2014**, *2*, 6895–6903.

[5] Krishnan, K.; Yamada, T.; Iwatsuki, H.; Hara, M.; Nagano, S.; Otsubo, K.; Sakata, O.; Fujiwara, A.; Kitagawa, H.; Nagao, Y. Influence of Confined Polymer Structure on Proton Transport Property in Sulfonated Polyimide Thin Films. *Electrochemistry* **2014**, *82*, 865–869.

[6] Matsui, J.; Miyata, H.; Hanaoka, Y.; Miyashita, T. Layered Ultrathin Proton Conductive Film Based on Polymer Nanosheet Assembly. *ACS Appl. Mater. Interfaces* **2011**, *3*, 1394–1397.

[7] Mauritz, K. A.; Moore, R. B. State of Understanding of Nafion. *Chem. Rev.* **2004**, *104*, 4535–4585.

[8] Schmidt-Rohr, K.; Chen, A. Q. Parallel Cylindrical Water Nanochannels in Nafion Fuel-Cell Membranes. *Nature Mater*. **2008**, *7*, 75–83.

[9] Gebel, G.; Diat, O. Neutron and X-ray Scattering: Suitable Tools for Studying Ionomer

Membranes. *Fuel Cells* **2005**, *5*, 261–276.

[10] Hsu, W. Y.; Gierke, T. D. Ion Transport and Clustering in Nafion Perfluorinated Membranes. *J. Membr. Sci*. **1983**, *13*, 307–26.

[11] Kreuer, K. D. On the Development of Proton Conducting Polymer Membranes for Hydrogen and Methanol Fuel Cells. *J. Membr. Sci*. **2001**, *185*, 29–39.

[12] Peng, H. C.; Wang, C. N.; Yeh, T. K.; Su, Y. C.; Pan, C.; Tseng, F. G. A high Efficient Micro-Proton Exchange Membrane Fuel Cell by Integrating Micro-Nano Synergic Structures. *J. Power Sources* **2014**, *225*, 277–285.

[13] More, K.; Borup, R.; Reeves, K. Identifying Contributing Degradation Phenomena in PEM Fuel Cell Membrane Electride Assemblies via Electron Microscopy. *ECS Trans.* **2006**, *3*,717–733.

[14] Paul, D. K.; Karan, K.; Docoslis, A.; Giorgi, J. B.; Pearce, J. Characteristics of Self-Assembled Ultrathin Nafion Films. *Macromolecules* **2013**, *46*, 3461–3475.

[15] Paul, D. K.; Fraser, A.; Karan, K. Towards the Understanding of Proton Conduction Mechanism in PEMFC Catalyst Layer: Conductivity of Adsorbed Nafion Films. *Electrochem. Commun.* **2011**, *13*, 774–777.

[16] Paul, D. K.; McCreery, R,; Karan, K. Proton Transport Property in Supported Nafion Nanothin Films by Electrochemical Impedance Spectroscopy. *J. Electrochem. Soc.* **2014**, *161*, 1395–1402.

[17] Paul, D. K.; Karan, K. Conductivity and Wettability Changes of Ultrathin Nafion Films Subjected to Thermal Annealing and Liquid Water Exposure. *J. Phys. Chem. C* **2014**, *118*, 1828–1835.

[18] Murthi, V. S.; Dura, J. A.; Satija, S.; Majkrzak, C. F. Water Uptake and Interfacial Structural Changes of Thin Film Nafion Membranes Measured by Neutron Reflectivity for PEM Fuel Cells. *ECS Trans*. **2008**, 16, 1471–1485.

[19] Dura, J. A.; Murthi, V. S.; Hartman, M.; Satija, S.; Majkrzak, C. F. Multilamellar Interface Structures in Nafion. *Macromolecules* **2009**, *42*, 4769–4774.

[20] Kim, S.; Dura, J. A.; Page, K. A.: Rowe, B. W.; Yager, K. G.; Lee, H. J.; Soles, C. L. Surface-Induced Nanostructure and Water Transport of Thin Proton-Conducting Polymer Films. *Macromolecules* **2013**, *46*, 5630–5637.

[21] Ogata, Y.; Kawaguchi, D.; Yamada, N.L.; Tanaka, K. Multistep Thickening of Nafion Thin Films in Water. *ACS Macro. Lett.* **2013**, *2*, 856–859.

[22] Wood, D. L.; Chlistunoff, J.; Majewski, J.; Borup, L. Nafion Structural Phenomena at Platinum and Carbon Interfaces. *J. Am. Chem. Soc.* **2009**, *131*, 18096–18104.

[23] Bass, M.; Beman, A.; Singh, A.; Konovalov, O.; Freger, V. Surface Structure of Nafion in Vapor and Liquid. *J. Phys. Chem. B* **2010**, *114*, 3784–3790.

[24] Bass, M.; Beman, A.; Singh, A.; Konovalov, O.; Freger, V. Surface-Induced Micelle Orientation in Nafion Films. *Macromolecules* **2011**, *44*, 2893–2899.

[25] Modestino, M. A.; Kusoglu, A.; Hexemer, A.; Weber, A. Z.; Segalman, R. A. Controlling Nafion Structure and Properties via Wetting Interactions. *Macromolecules* **2012**, *45*, 4681–4688.

[26] Modestino, M. A.; Paul, D. K.; Dishari, S.; Petrina, S. A.; Allen, F.; Hickner, M. A.; Karan, K.; Segalman, R. A.; Weber, A. Z. Self-Assembly and Transport Limitations in Confined Nafion Films. *Macromolecules* **2013**, *46*, 867–873.

[27] Kusoglu, A.; Kushner, D.; Paul, D. K.; Karan, K.; Hickner, M. A.; Weber, A. Z. Impact of Substrate and Processing on Confinement of Nafion Thin Films. *Adv. Funct. Mater.* **2014**, *24*, 4763–4774.

[28] Eastman, S. A.; Kim, S.; Page, K. A.; Rowe, B. W.; Kang, S.; Soles, C. L. Effect of Confinement on Structure, Water Solubility, and Water Transport in Nafion Thin Films. *Macromolecules* **2012,** *45***,** 7920–7930.

[29] Nagao, Y. Proton Transport Property of Nafion Thin Films on MgO(100) with Anisotropic Molecular Structure. *e-J. Surf. Sci. Nanotechnol.* **2012**, *10* 114–116.

[30] Nagao, Y. Highly Oriented Sulfonic Acid Groups in a Nafion Thin Film on Si Substrate. *J. Phys. Chem. C* **2013**, *117*, 3294–3297.

[31] Hasegawa, T. A Novel Measurement Technique of Pure Out-of-plane Vibrational Modes in Thin Films on a Nonmetallic Material with No Polarizer. *J. Phys. Chem. B* **2002**, *106*, 4112–4115.

[32] Hasegawa, T.; Matsumoto, L.; Kitamura, S.; Amino, S.; Katada, S.; Nishijo, J. Optimum Condition of Fourier Transform Infrared Multiple-Angle Incidence Resolution Spectrometry for Surface Analysis. *Anal. Chem*. **2002**, *74*, 6049–6054.

[33] Hasegawa, T. Advanced Multiple-angle Incidence Resolution Spectrometry for Thin-layer Analysis on a Low-refractive-index Substrate. *Anal. Chem.* **2007**, *79*, 4385–4389.

[34] Hasegawa, T.; Itoh, Y.; Kasuya, A. A. Experimental Optimization of P-polarized MAIR Spectrometry Performed on a Fourier Transform Infrared Spectrometer. *Anal. Sci*. **2008**, *24*, 105–109.

[35] Siroma, Z.; Kakitubo, R.; Fujiwara, N.; Ioroi, T.; Yamazaki, S.; Yasuda, K. Depression of Proton Conductivity in Recast Nafion Film Measured on Flat Substrate. *J. Power Sources* **2009**, *189*, 994–998.

[36] Kongkanand, A. Interfacial Water Transport Measurements in Nafion Thin Films Using a Quartz-Crystal Microbalance. *J. Phys. Chem. C* **2011**, *115*, 11318–11325.

[37] Abuin, G. C.; Fuertes, M. C.; Corti, H. R. Substrate Effect on the Swelling and Water Sorption of Nafion Nanomembranes. *J. Membr. Sci*. **2013**, *428*, 507–515.

[38] Dishari, S. K.; Hickner, M. A. Antiplasticization and Water Uptake of Nafion Thin Films. *ACS Macro. Lett.* **2012**, *1*, 291–295.

[39] Parkinson, C. R.; Walker, M.; McConville, C. F. Reaction of Atomic Oxygen with a Pt(111) Surface: Chemical and Structural Determination Using XPS, CAICISS and LEED.

Surf. Sci. **2003**, *545*, 19–33.

[40] Gruger, A.; Regis, A.; Schmatko, T.; Colomban, P. Nanostructure of Nafion Membranes at Different States of Hydration an IR and Raman Study. *Vib. Spectrosc.* **2001**, *26*, 215–225.

[41] Danilczuk, M.; Lin, L.; Schlick, S.; Hamrock, S. J.; Schaberg, M. S. Understanding the Fingerprint Region in the Infra-red Spectra of Perfluorinated Ionomer Membranes and Corresponding Model Compounds: Experiments and Theoretical Calculations. *J. Power Sources* **2011**, *196*, 8216–8224.

[42] Davis, E. M.; Stafford, C. M.; Page, K. A. Elucidating Water Transport Mechanisms in Nafion Thin Films. *ACS Macro Lett*. **2014**, *3*, 1029–1035.

[43] Kendrick, I.; Kumari, D.; Yakaboski, A.; Dimakis, N.; Smotkin, E. S. Elucidating the Ionomer-electrified Metal Interface. *J. Am. Chem. Soc.* **2010**, *132*, 17611–17616.

[44] Zeng, J.; Jean, D. I.; Ji, C.; Zou, S. In Situ Surface-Enhanced Raman Spectroscopic Studies of Nafion Adsorption on Au and Pt Electrodes. *Langmuir* **2012**, *28*, 957– 964.

[45] Malevich, D.; Zamlynny, V.; Sun, S.-G.; Lipkowski, J. In situ Infrared Reflection Absorption Spectroscopy Studies of the Interaction of Nafion® with the Pt Electrode Surface. *Z. Phys. Chem.* **2003**, *217*, 513–525.

[46] Korzeniewski, C.; Snow, D. E.; Basnayake, R. Transmission Infrared Spectroscopy as a Probe of Nafion Film Structure: Analysis of Spectral Regions Fundamental to Understanding Hydration Effects. *Appl. Spectrosc*. **2006**, *60*, 599–604.

[47] Yamaguchi, M.; Ohira, A. Vibrational Analysis of Side Chain Model Compounds of Perfluorinated Alkyl Sulfonic Acid Ionomers. *J. Phys. Chem. A* **2012**, *116*, 10850–10863.

[48] Warren, D. S.; McQuillan, A. J. Infrared Spectroscopic and DFT Vibrational Mode Study of Perfluoro(2-ethoxyethane) Sulfonic Acid (PES), a Model Nafion Side-chain Molecule. *J. Phys. Chem. B* **2008**, *112*, 10535–10543.

[49] Ludvigsson, M.; Lindgren, J.; Tegenfeldt, J. FTIR Study of Water in Cast Nafion Films. *Electrochim. Acta* **2000**, *45*, 2267–2271.

[50] Malek, K.; Mashio, T.; Eikerling, M. Microstructure of Catalyst Layers in PEM Fuel Cells Redefined: A Computational Approach. *Electrocatal*. **2011**, *2*, 141–157.

[51] Yagi, I.; Inokuma, K.; Kimijima, K.; Notstu, H. Molecular Structure of Buried Perfluorosulfonated Ionomer/Pt Interface Probed by Vibrational Sum Frequency Generation Spectroscopy. *J. Phys. Chem. C* **2014**, *118*, 26182–26190.

TOC

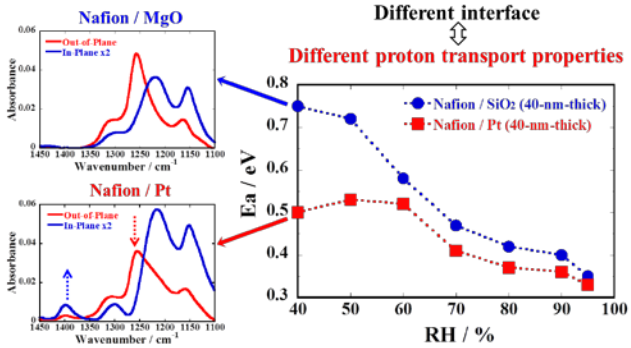
Nafion / MgO
Out of Plane
In Plane x2
Absorbance
Wavenumber / cm-1
Nafion / Pt
Different interface
Different proton transport properties
Nafion / SiO2 (40-nm-thick)
Nafion / Pt (40-nm-thick)
Ea / eV
RH / %